

Comparative Study of Different Numerical Models for Vehicle–Bridge Interaction Analysis

Qiling Zou*, Lu Deng^{†§}, Tieding Guo* and Xinfeng Yin[‡]

**College of Civil Engineering, Hunan University
Changsha, Hunan 410082, China*

*†Key Laboratory for Wind
and Bridge Engineering of Hunan Province
Hunan University
Changsha, Hunan 410082, China*

*‡School of Civil Engineering and Architecture
Changsha University of Science and Technology
Changsha, Hunan 410004, China
§dengl@hnu.edu.cn*

Received 9 March 2015

Accepted 15 August 2015

Published 6 October 2015

In this paper, a comprehensive comparative study on several existing vehicle–bridge interaction (VBI) models is presented with the aim to provide a useful reference to the selection of vehicle and bridge models when conducting the VBI simulation. A simply-supported slab-on-girder highway bridge and the AASHTO HS20-44 vehicle are adopted in the numerical analysis. The bridge is modeled as an Euler–Bernoulli beam, grillage, plate-and-beam system and solid-element system, respectively, while the vehicle is modeled as a moving-force, moving-mass and spring-damper-mass (SDM) system, respectively. Other factors, including the road roughness and the contact condition between the vehicle tire and bridge, are also considered. The effects of different VBI models on the bridge responses are studied and the results from different models are compared in terms of their accuracy, efficiency and suitability. The results show that the accuracy of different types of bridge responses calculated varies with the number of bridge vibration modes used in the simulation. It is also found that the type of element used in the bridge model and the vehicle tire model both have a larger impact on the bridge acceleration than bridge deflection.

Keywords: Vehicle–bridge interaction; numerical model; impact factor; dynamic load coefficient; road roughness.

§Corresponding author.

1. Introduction

In the past few decades, the dynamic interactions between moving vehicles and bridges have been extensively studied. The maximum dynamic response of a bridge induced by moving vehicles is usually larger than the maximum static response subjected to the corresponding static vehicle loads. It is widely accepted that this dynamic increment is influenced by many factors, including the bridge span length or natural frequency, road surface roughness, vehicle suspension system, vehicle speed, gross vehicle weight, etc. Due to the complexity of the vehicle–bridge interaction (VBI) problem and the lack of field test data which are usually inconvenient and expensive to obtain, many numerical models have been developed to simulate the behavior of the VBI system. A VBI system generally contains three parts: the bridge model, the vehicle model and the road roughness model.

Depending on the complexity, the bridge model can usually be categorized into three groups. The one-dimensional (1D) models are the simplest and are usually modeled as a single Euler–Bernoulli beam which ignores the torsional and transverse vibration modes of the bridge.^{1–3} The two-dimensional (2D) models are usually implemented with the grillage method⁴ or the four-node plate/shell elements.^{5,6} The three-dimensional (3D) models generally adopt the eight-node solid elements^{7,8} or are composed of an assemblage of shell and beam elements.^{9,10}

The vehicle is generally simulated as one of the following: moving-force, moving-mass, a spring-damper-mass (SDM) system and a full-scale finite-element (FE) model. The moving-force model, which is the simplest among all four vehicle models, may produce dynamic bridge responses with satisfactory accuracy under certain circumstances while the interaction between the vehicle and bridge cannot be considered. The moving-mass model can account for the inertia effect of the vehicle; however, it fails to consider the bouncing action of the vehicle induced by the road roughness.¹¹ The widely-used SDM models overcome these drawbacks and simulate the VBI more realistically while maintaining an acceptable level of complexity. In the SDM models, vehicle bodies and axles are represented by rigid bodies with masses, and all components are connected by springs and dampers. The SDM models can also be classified into three groups according to their dimension and complexity. The 1D model (also called the quarter vehicle model) only takes into consideration the vertical movement of the vehicle axle and the vehicle body;^{12,13} the 2D model (also called the half vehicle model) considers the motion in both directions in the vertical plane;^{2,14} and the 3D model considers the motion in all three dimensions in the space.^{5,7,15} Based on the type of contact between the bridge and vehicle tire, the SDM models can be further classified into the single-point-contact (SPC) model and the patch-contact or multiple-point-contact (MPC) model,^{16,17} where the latter takes into account the more realistic contact behavior of the tire. Very sophisticated FE vehicle models, in which the vehicle components are modeled by different elements, have also been used by some researchers. Nevertheless, this type of FE vehicle models is not widely used due to their complexity and relatively low computational

efficiency, especially when the simulation of random traffic flow of large volume is needed.¹⁸

Road roughness is recognized as one of the most important excitation sources in the vehicle–bridge interacted vibrations. Some researchers considered the difference of the roughness profiles in the transverse direction,^{5,6,19} while others assumed that the roughness profiles are fully-correlated (FC).⁸

To date, little work has been devoted to compare the accuracy efficiency and suitability of different VBI models comprehensively for different circumstances. The main purpose of this paper is therefore to provide researchers with a detailed cross-comparison of the existing VBI models focusing on the influence on the bridge responses. It is hoped that this paper can provide a better understanding of different VBI models and provide a comprehensive reference in selecting suitable models.

In this study, different VBI models are first presented. The bridge is modeled by a discretized Euler–Bernoulli beam, grillage, assemblage of shell and beam elements and solid elements, respectively. The vehicle is modeled as a moving-force, moving-mass and SDM model, respectively. The SDM model incorporates both the SPC and MPC tire models. The road surface roughness is simulated by the power spectral density (PSD) provided by ISO 8608,²⁰ and both FC and partially-correlated (PC) roughness profiles are considered. Different types of bridge responses and the tire contact forces are calculated and compared. The influence of different components of VBI models, including the bridge model, vehicle model and road roughness model, on the behavior of the VBI system are studied focusing on the bridge responses. The computational efficiency of different VBI models is also discussed.

2. Analytical Model

2.1. Bridge

A typical two-lane simply-supported slab-on-girder concrete bridge designed in accordance with the AASHTO specifications is selected in the present study.²¹ The bridge, consisting of five identical AASHTO Type-III girders with a girder spacing of 2.13 m, has a span length of 24.384 m, roadway width of 9.75 m and bridge deck thickness of 0.2 m. The cross section of the bridge is shown in Fig. 1.

Four different bridge models are created based on the geometry and material properties of the bridge and are briefly introduced below.

- (i) The single-beam model: The entire bridge is modeled as a single discretized Euler–Bernoulli planar beam in which each node is associated with three degrees of freedom (DOFs), including two translational DOFs and one rotational DOF. It is known that this model can only accurately deal with symmetric loading cases.²²
- (ii) The grillage model: The entire bridge is modeled by longitudinal and transverse Euler–Bernoulli beam elements using the grillage method.⁴ Each node of the

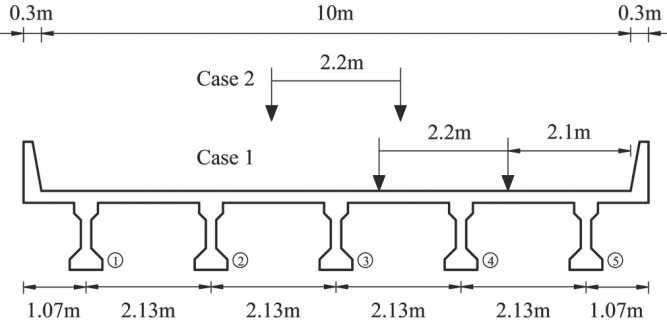


Fig. 1. Bridge cross section and loading cases.

- beam element is associated with six DOFs, including three translational and three rotational DOFs.
- (iii) The shell-and-beam model: The bridge deck is modeled by shell elements while the girders and diaphragms are modeled by beam elements.^{9,10} Each node of the shell element is associated with five DOFs, including three translational and two rotational DOFs, while each node of the beam element has six DOFs, including three translational and three rotational DOFs.¹⁰
 - (iv) The solid-element model: The entire bridge is modeled with eight-node solid elements, each node having three translational DOFs.⁷ The shape function of the eight-node solid elements is linear for each translational DOF.

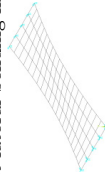
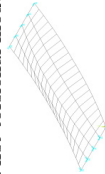
The theories for different models can be found in the corresponding references and will not be introduced in detail here. It should be noted that only the superstructure is modeled while the abutments and columns are considered by setting appropriate support conditions.

The natural frequencies and vibration mode shapes are often used when studying the dynamic behavior of a bridge.²³ Modal analysis is performed for the four bridge models created and the results of the first four natural frequencies and corresponding mode shapes are shown in Table 1. It can be seen that the first bending modes for all four bridge models agree well with each other. However, small difference can still be observed for some vibration modes, e.g. the second vertical bending mode and the bidirectional bending mode, between different bridge models.

2.2. Vehicle

The AASHTO HS20-44 truck, with static weights of 17.8, 71.2 and 71.2 kN for the three axles, respectively, is used in the numerical analysis. The truck is modeled as a moving-force, moving-mass and SDM vehicle model, respectively, as shown in Figs. 2–4, respectively. Two different tire models, i.e. the SPC and MPC tire models, are used for the SDM truck model. For convenience, the corresponding SDM models will be referred to as the SPC-SDM vehicle model and MPC-SDM vehicle model

Table 1. The first four vibration modes of different bridge models.

Overall mode	Bridge models			
	Single-beam	Grillage	Shell-and-beam	Solid-element
1	 $f_1 = 4.46$ Hz	 $f_1 = 4.51$ Hz First vertical bending mode	 $f_1 = 4.67$ Hz First vertical bending mode	 $f_1 = 4.60$ Hz
2	 $f_2 = 17.17$ Hz Second vertical bending mode	 $f_2 = 5.52$ Hz First lateral bending mode	 $f_2 = 6.15$ Hz First torsional mode	 $f_2 = 6.23$ Hz First torsional mode
3	 $f_3 = 36.56$ Hz Third vertical bending mode	 $f_3 = 7.21$ Hz First torsional mode	 $f_3 = 11.58$ Hz Bidirectional bending mode	 $f_3 = 11.19$ Hz Bidirectional bending mode
4	 $f_4 = 37.76$ Hz First axial mode	 $f_4 = 12.20$ Hz Bidirectional bending mode	 $f_4 = 17.65$ Hz Second vertical bending mode	 $f_4 = 15.09$ Hz First lateral bending mode

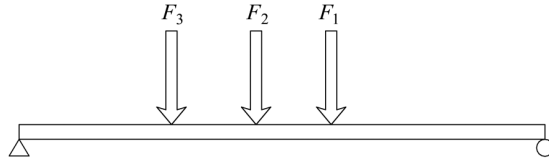


Fig. 2. The moving-force model.

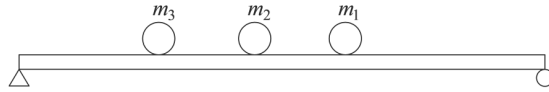


Fig. 3. The moving-mass model.

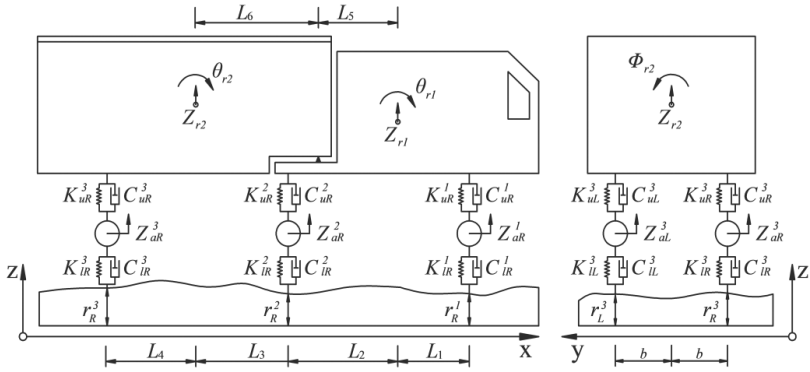


Fig. 4. The SPC-SDM vehicle model for the HS20-44 truck under study.

hereafter, respectively. The MPC-SDM model is identical to the SPC-SDM model except that each tire is modeled with multiple identical springs and dampers instead of a single spring and damper in the SPC-SDM model with the purpose to simulate the patch contact, which covers a length of 0.24 m,⁵ between the tire and the road, as illustrated in Fig. 5. Results from a sensitivity analysis show that using six springs and dampers to model the tire can lead to satisfactory convergence of the dynamic response of both the bridge and the vehicle.

The moving-force model consists of three or six constant axle forces which are equal to the static axle or wheel weights of the corresponding SPC-SDM model. As for the moving-mass model, the value of each mass is equal to the corresponding force in the moving-force model divided by the acceleration of gravity, i.e. 9.81 m/s². The spacings between the adjacent forces or masses are in accordance with the geometry of the 3D SPC-SDM model shown in Fig. 4. The parameters of the 3D SDM model

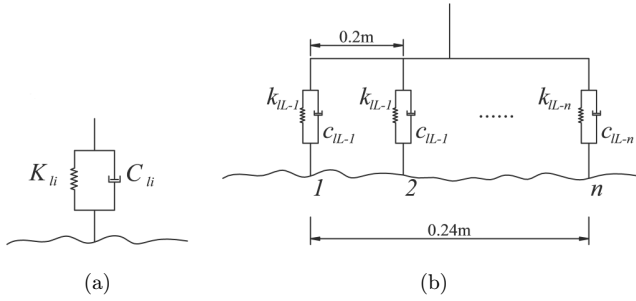


Fig. 5. The tire models: (a) SPC model; and (b) MPC model.

Table 2. The parameters of the SPC-SDM vehicle model for the HS20-44 truck under study.

Main parameters	Value
Mass of truck body 1 (kg)	2612
Pitching moment of inertia of truck body 1 (kg·m ²)	8543.88
Rolling moment of inertia of truck body 1 (kg·m ²)	2021.52
Mass of truck body 2 (kg)	26,113
Pitching moment of inertia of truck body 2 (kg·m ²)	181,216.3
Rolling moment of inertia of truck body 2 (kg·m ²)	33,153.26
Mass of the first axle suspension (kg)	489.6
Upper spring stiffness of the first axle (N/m)	242,604
Upper damper coefficient of the first axle (N·s/m)	2189.56
Lower spring stiffness of the first axle (N/m)	875,082
Lower damper coefficient of the first axle (N·s/m)	2000
Mass of the second axle suspension (kg)	808.4
Upper spring stiffness of the second axle (N/m)	1,903,172
Upper damper coefficient of the second axle (N·s/m)	7882.44
Lower spring stiffness of the second axle (N/m)	3,503,307
Lower damper coefficient of the second axle (N·s/m)	2000
Mass of the third axle suspension (kg)	652.5
Upper spring stiffness of the third axle (N/m)	1,969,034
Upper damper coefficient of the third axle (N·s/m)	7181.78
Lower spring stiffness of the third axle (N/m)	3,507,429
Lower damper coefficient of the third axle (N·s/m)	2000
L_1 (m)	1.698
L_2 (m)	2.569
L_3 (m)	1.984
L_4 (m)	2.283
L_5 (m)	2.215
L_6 (m)	2.338
b (m)	1.1

with 11 independent DOFs are listed in Table 2.⁸ For the 2D single-beam model, the parameters of the vehicle related to the lateral dimension (e.g. the rolling moment of inertia) are either ignored or combined to deduce the planar SDM model, which has only six independent DOFs but the same weight as the 3D SDM model.

2.3. Road roughness

Road roughness is generally regarded as the most important source of excitation in the VBI and can be included only when the SDM vehicle models are used. Road roughness profiles can be represented with a zero-mean normal stationary random process described by a PSD. Based on the work of Oliva *et al.*,⁶ two correlated parallel road roughness profiles can be generated by

$$r_1(x) = \sum_{i=1}^N \sqrt{2G(n_{1i})\Delta n} \cos(2\pi n_{1i}x + \phi_{1i}), \quad (2.1a)$$

$$r_2(x) = \sum_{i=1}^N \sqrt{2(G(n_{1i}) - G_x(n_{1i}))\Delta n} \cos(2\pi n_{1i}x + \phi_{1i}) + \sum_{i=1}^N \sqrt{2G(n_{2i})\Delta n} \cos(2\pi n_{2i}x + \phi_{2i}), \quad (2.1b)$$

$$n_{ji} = n_l + (i - 1)\Delta n + \frac{j}{2}\Delta n, \quad j = 1, 2; i = 1, 2, \dots, N, \quad (2.1c)$$

where n_{ji} is the spatial frequency (cycle/m); ϕ_{1i} and ϕ_{2i} are two independent random phase angles uniformly distributed from 0 to 2π ; N is the number of the frequencies between n_l and n_u , which are the lower and upper cut-off frequencies, respectively; $\Delta n = (n_u - n_l)/N$ is the frequency interval; $G(\cdot)$ is the one-sided PSD function specified in the ISO 8608 (m^3/cycle)²⁰; and $G_x(\cdot)$ is the cross-PSD which describes the correlation of two road roughness profiles in the frequency domain (m^3/cycle).⁶

In this study, four road roughness classes, i.e. very good, good, average and poor, based on the different values of PSD, are selected to investigate the effect of the

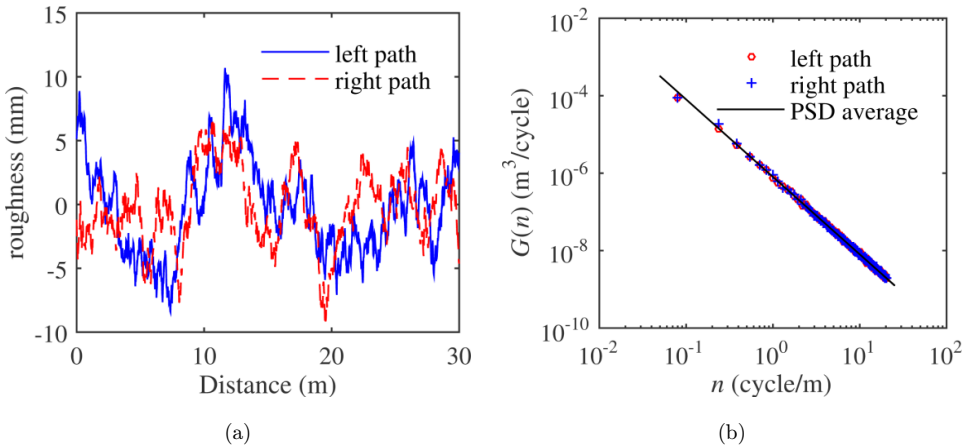


Fig. 6. (Color online) Average-class parallel road roughness profiles: (a) Roughness; and (b) one-sided PSD.

road surface condition (RSC) on the VBI.⁴ Meanwhile, both FC roughness profiles, which can be generated by Eq. (2.1a), and the PC roughness profiles, which can be generated by Eqs. (2.1a) and (2.1b), are taken into account. An example of two PC average-class roughness profiles and their PSD are shown in Fig. 6.

3. VBI System

The equation of motion for a bridge can be written as

$$[M_b]\{\ddot{d}_b\} + [C_b]\{\dot{d}_b\} + [K_b]\{d_b\} = [N]^T\{F_b\}, \quad (3.1)$$

where $[M_b]$, $[C_b]$ and $[K_b]$ are the mass, damping and stiffness matrices of the bridge, respectively; $\{d_b\}$, $\{\dot{d}_b\}$ and $\{\ddot{d}_b\}$ are the vectors of displacement, velocity and acceleration of the bridge, respectively; $[N]$ is the shape function matrix of the bridge deck elements; and $\{F_b\}$ is a vector of the wheel-bridge contact forces acting on the bridge. The method for assembling the VBI system varies according to the different vehicle models used.

3.1. The moving-force model

When the vehicle is modeled as several constant forces, which can be directly substituted into $\{F_b\}$ in Eq. (3.1), the motion of the vehicle is neglected, and the terms $[M_b]$, $[C_b]$ and $[K_b]$ in Eq. (3.1) are all time-independent. In this case, the response of the bridge can be easily obtained by solving Eq. (3.1).

3.2. The moving-mass model

In addition to the gravity forces, the inertial forces of the masses in the moving-mass model should also be included in the force vector $\{F_b\}$ acting on the bridge, as expressed below:

$$\{F_b\} = -\{M_{vi}g + M_{vi}\ddot{d}_{vi}\}, \quad (3.2)$$

where M_{vi} is the mass of the i th mass; and \ddot{d}_{vi} is the acceleration of the i th mass. Substituting this relationship into Eq. (3.1) and employing the relationship between the displacement of the i th mass d_{vi} and bridge displacement $\{d_b\}$ (See Ref. 24) yield the following:

$$\begin{aligned} & \left[M_b + \sum_{i=1}^k M_{vi}\{N_i\}^T\{N_i\} \right] \{\ddot{d}_b\} + \left[C_b + 2v \sum_{i=1}^k M_{vi}\{N_i\}^T\{N_{ix}\} \right] \{\dot{d}_b\} \\ & + \left[K_b + v^2 \sum_{i=1}^k M_{vi}\{N_i\}^T\{N_{ixx}\} + \dot{v} \sum_{i=1}^k M_{vi}\{N_i\}^T\{N_{ix}\} \right] \{d_b\} \\ & = -g \sum_{i=1}^k M_{vi}\{N_i\}^T, \end{aligned} \quad (3.3)$$

where $\{N_i\}$, $\{N_{ix}\}$ and $\{N_{ixx}\}$ are the shape function related to the position of the i th mass, and the first and second partial derivatives with respect to x (the longitudinal direction of the bridge), respectively; v and \dot{v} are the speed and acceleration of the vehicle, respectively. Compared with Eq. (3.1), those new terms in Eq. (3.3) are all time-dependent. These terms are calculated once the vehicle position on the bridge is determined and are updated at each time step.

3.3. The SDM model

As mentioned before, the SDM vehicle model can account for the DOFs of the vehicle. The vibrations of the vehicle and the bridge interact through the vehicle tires which are simulated as springs and dampers. Using the displacement relationship and the interaction force relationship at the contact points, the vehicle–bridge coupled system can be established by combining the equations of motion of both the bridge and the vehicle,⁷ as shown below:

$$\begin{aligned} & \begin{bmatrix} M_b & \\ & M_v \end{bmatrix} \begin{Bmatrix} \ddot{d}_b \\ \ddot{d}_v \end{Bmatrix} + \begin{bmatrix} C_b + C_{b-b} & C_{b-v} \\ C_{v-b} & C_v \end{bmatrix} \begin{Bmatrix} \dot{d}_b \\ \dot{d}_v \end{Bmatrix} \\ & + \begin{bmatrix} K_b + K_{b-b} & K_{b-v} \\ K_{v-b} & K_v \end{bmatrix} \begin{Bmatrix} d_b \\ d_v \end{Bmatrix} = \begin{Bmatrix} F_{b-r} \\ F_{v-r} + F_v^G \end{Bmatrix}, \end{aligned} \quad (3.4)$$

where the subscripts b , v and r denote the bridge, vehicle and road roughness, respectively; $\{F_v^G\}$ is the vector of gravity force of the vehicle; and C_{b-b} , C_{b-v} , C_{v-b} , K_{b-b} , K_{b-v} , K_{v-b} , F_{b-r} and F_{v-r} are due to the wheel–road contact forces, which are all time-dependent and will change with the position of the vehicle on the bridge, and thus should be updated at each time step.^{7,8} The only difference between the SPC-SDM and MPC-SDM vehicle models lies in the terms related to the damping and stiffness of the vehicle tires in Eq. (3.4).

Based on the methodology described above, different MATLAB codes have been developed to simulate the VBI for different bridge and vehicle models adopted. To simplify the bridge model and therefore reduce the computational effort, the modal superposition technique is used. The equations of motion of the VBI system are solved using the Newmark- β method.²⁵

3.4. Model validation

In order to validate the VBI methodology described in this paper, several benchmark tests involving different vehicle and bridge models used in previous studies have been conducted. The moving-force and moving-mass problems are taken from Ref. 26 and the SDM vehicle model with the single-beam bridge model is modeled according to Ref. 13. Meanwhile, the results of the cases with the SDM vehicle model and the bridge simulated as grillage, shell-and-beam and solid models, respectively, are compared with the field test data from Ref. 27. The details of modeling are not

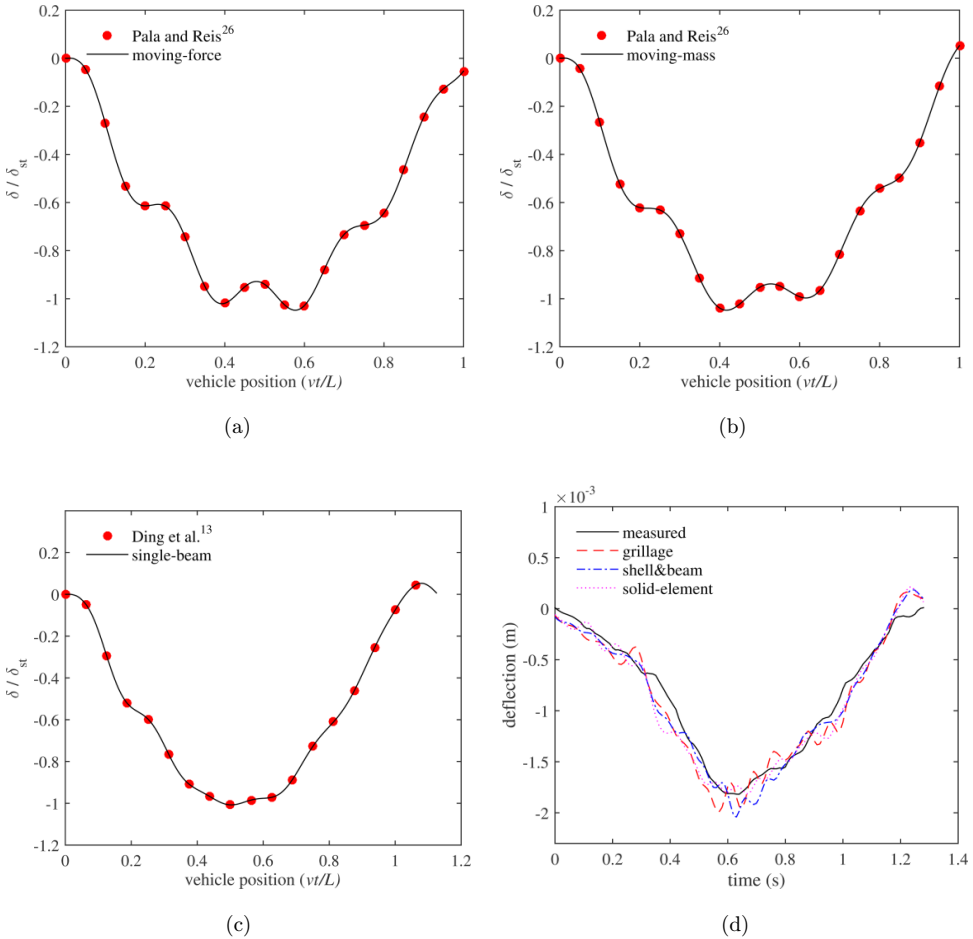


Fig. 7. (Color online) Vertical displacement at the mid-span in the benchmark tests: (a) Moving-force vehicle model and single-beam bridge model, $v = 5$ m/s; (b) moving-mass vehicle model and single-beam bridge model, $v = 5$ m/s; (c) SDM vehicle model and single-beam bridge model, $v = 25$ m/s; and (d) SDM vehicle model and the other three bridge models, $v = 17.88$ m/s.

presented here for the sake of brevity while further information can be found in the reference papers. Figure 7 shows the bridge deflection time histories at the mid-span. A very close match can be observed between the results from the proposed methods and those from the reference papers, indicating that the methodology developed in this paper can accurately simulate the dynamic behavior of the VBI system.

4. Numerical Study

In this section, the influence of different components of the VBI model, including the bridge model, vehicle model and road roughness model, on the bridge responses is

discussed separately. The bridge responses considered include the deflection, bending strain and vertical acceleration, which have been commonly selected in other studies.²⁸ In addition, since the tire–bridge contact forces have a significant influence on the local impact on the bridge deck and can be treated as the external forces to the bridge, they are also taken into account in the related subsections.¹³

Two commonly used parameters in bridge design, i.e. the dynamic impact factor (IM)²⁹ and the dynamic load coefficient (DLC),¹³ are also adopted. The IM has been widely used to assess the bridge dynamic response, and is defined as

$$\text{IM} = \frac{R_d - R_s}{R_s}, \quad (4.1)$$

where R_d denotes the maximum dynamic response and R_s denotes the maximum static response. The DLC is used to indicate the magnitude of the dynamic axle loads and is defined as

$$\text{DLC} = \frac{P_d - P_s}{P_s}, \quad (4.2)$$

where P_d and P_s denote the maximum dynamic and static axle loads, respectively.

Before presenting the results of the dynamic responses, the results of quasi-static responses of all girders are given in Table 3. These results were obtained under the case in which each vehicle model crosses the corresponding bridge model at a crawling speed (1.2 km/h) with perfectly smooth road profile. It should be noted that since unsymmetrical loading cases cannot be considered in the single-beam model, no results of case 1 are reported for the single-beam model in Table 3. The results in Table 3 show that different bridge models exhibit great similarities for the quasi-static deflections of five girders under each case, indicating that these models are statically equivalent. These results also reveal that different vehicle models do not cause a significant difference on the bridge deflection at very slow vehicle speeds.

Very high IMs are usually observed for exterior girders (i.e. girder 1 and girder 5)¹⁸ and these IM values have no practical meaning because they correspond to small static and dynamic responses.²⁹ Therefore, the girders that have the maximum static bridge response under the corresponding loading cases, i.e. girder 4 under case 1 and girder 3 under case 2, are selected for the result analysis of the IM.

4.1. Effect of the bridge model

4.1.1. The number of bridge vibration modes

Since the modal superposition technique is adopted to obtain the bridge responses, the contribution of each mode can be easily evaluated. The SPC-SDM vehicle model and FC road roughness profiles are adopted here.

(i) Deflection of bridge: The first 60 modes are used to calculate the deflection of the bridge in this study. The results show that the first few modes contribute the most to the bridge mid-span deflection. For the grillage, shell-and-beam and

Table 3. The maximum quasi-static deflection at bridge mid-span under cases 1 and 2.

Bridge model	Vehicle model	Deflection (mm)													
		Girder 1		Girder 2		Girder 3		Girder 4		Girder 5					
		Case 1	Case 2	Case 1	Case 2	Case 1	Case 2	Case 1	Case 2	Case 1	Case 2				
Single-beam	Moving-force														
	Moving-mass														
	SDM					3.29 (case 2)	3.29 (case 2)	3.29 (case 2)							
Grillage	Moving-force	1.33	2.26	2.15	2.96	3.05	3.31	3.55	2.96	3.48	2.26				
	Moving-mass	1.33	2.26	2.15	2.96	3.05	3.31	3.55	2.96	3.48	2.26				
	SDM	1.33	2.26	2.15	2.96	3.05	3.31	3.55	2.96	3.48	2.26				
Shell-and-beam	Moving-force	1.33	2.26	2.15	2.96	3.05	3.31	3.55	2.96	3.48	2.26				
	Moving-mass	1.33	2.26	2.15	2.96	3.05	3.31	3.55	2.96	3.48	2.26				
	SDM	1.33	2.26	2.15	2.96	3.05	3.31	3.55	2.96	3.48	2.26				
Solid-element	Moving-force	1.37	2.24	2.17	2.94	3.03	3.30	3.50	2.94	3.42	2.24				
	Moving-mass	1.37	2.24	2.17	2.94	3.03	3.30	3.50	2.94	3.42	2.24				
	SDM	1.37	2.24	2.17	2.94	3.03	3.30	3.50	2.94	3.42	2.24				

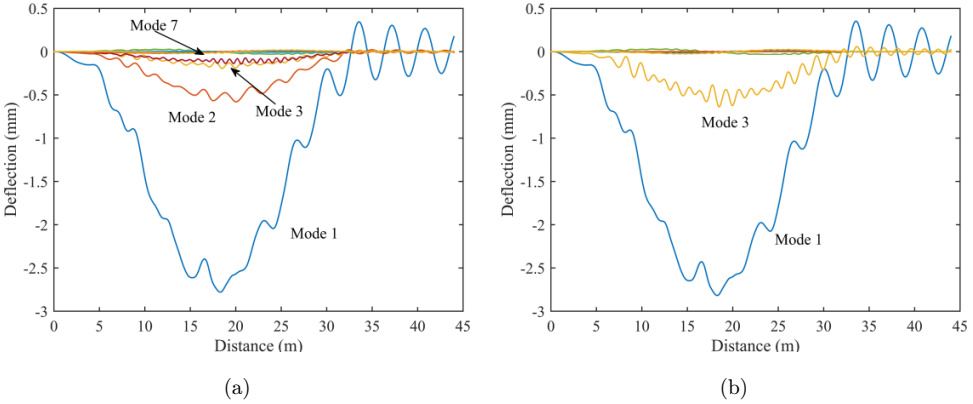


Fig. 8. (Color online) Modal contributions to the total bridge deflection with the SDM vehicle model traveling at 60 km/h under good RSC (solid-element model): (a) Case 1; and (b) case 2.

solid-element models, the contribution of the first 10 modes account for around 97% of the total deflection. Take the solid-element model as an example for illustration. Figure 8 shows the contribution of each mode to the total mid-span deflection of corresponding girder under cases 1 and 2, respectively. The distance between the vehicle’s first axle and the bridge entrance, instead of time, is used as the x -axis. If the truck crosses the bridge along the right lane (case 1), all vibration modes will be excited, as shown in Fig. 8(a). However, when the truck crosses the bridge along the centerline of the roadway (case 2), all modes that are asymmetric about the centerline are not excited. It is noted that mode 3, which is a bidirectional flexural mode, accounts for a considerable proportion of the total response in case 2. Table 4 shows the contributions of the bidirectional flexural modes of the three bridge models (mode 4 for the grillage model, mode 3 for the shell-and-beam and solid-element models) to the total mid-span deflection under case 2 considering different vehicle speeds and RSCs. It can be seen that the largest contribution can reach nearly 20%. For the single-beam model, the contribution of the first flexural mode usually accounts for 99% of the total deflection. These results show that even for the case

Table 4. Contributions of the bidirectional modes to the total mid-span deflection under case 2 (%).

v (km/h)	Grillage			Shell-and-beam			Solid-element		
	Poor	Average	Good	Poor	Average	Good	Poor	Average	Good
30	14.4	13.5	12.5	16.6	15.6	15.3	16.9	16.1	15.7
45	15.8	14.4	13.1	17.1	16.2	15.8	16.9	16.6	16.1
60	14.9	13.7	12.7	16.4	16.3	15.4	16.3	16.6	15.7
75	14.7	13.6	11.9	18.3	17.1	15.3	19.1	18.1	16.0
90	18.3	15.3	12.6	19.1	17.4	14.9	19.3	17.4	15.6
105	16.1	15.3	13.6	18.2	18.2	16.6	19.0	18.8	17.4
120	15.0	13.7	12.6	18.2	16.9	15.6	19.3	18.2	16.3

with the truck running along the centerline of the roadway, it is not sufficient to model the bridge with a single beam since the contributions of the transverse modes can be significant.¹⁰ In reality, the asymmetric modes can even be excited under the symmetric loading scenarios due to the variation of the road profile in the lateral direction. Therefore, the single-beam model may not be able to predict bridge responses with satisfactory accuracy, especially for bridges with large width-to-span ratio and under asymmetric loading conditions.

(ii) Bending strain of bridge: Although employing the first few modes can usually lead to sufficiently accurate prediction of bridge deflection, incorporation of higher modes is necessary to ensure the accuracy of the predicted bending strain of the bridge. Figure 9 shows the contribution, in percentage, of each of the first 60 modes to the maximum strain at the bridge mid-span for different bridge models under different loading cases at a vehicle speed of 75 km/h. It can be seen that approximately 20 modes are required to reach sufficiently accurate prediction of the bending strain for all three models (i.e. the grillage, shell-and-beam and solid-element models) under the two loading cases considered. A careful examination reveals that the

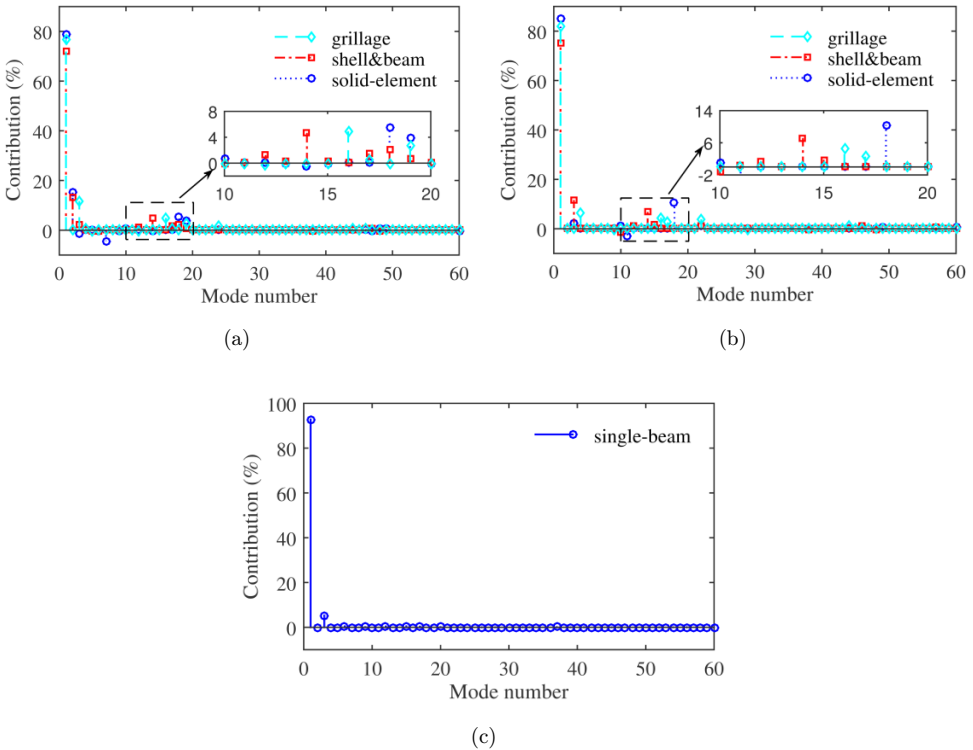


Fig. 9. (Color online) Modal contributions of the first 60 modes to the maximum mid-span bending strain (75 km/h, average RSC): (a) Case 1; (b) case 2; and (c) single-beam model.

highest peak lying between the 10th and 20th modes corresponds to the third vertical flexural mode for all three different bridge models, namely mode 16 for the grillage model (39.92 Hz), mode 14 for the shell-and-beam model (37.86 Hz) and mode 18 for the solid-element model (37.58 Hz) (see zoom-in graphs in Figs. 9(a) and 9(b)). The third vertical flexural mode is also obvious for the single-beam model, as shown in Fig. 9(c).

(iii) Acceleration of bridge: Figure 10 depicts the PSD spectra of the vertical acceleration of bridges at the mid-span under case 2 with an average RSC. The first peak observed in all figures, which corresponds to a frequency around 4.5 Hz, represents the fundamental vibration mode of the bridge. In addition, the

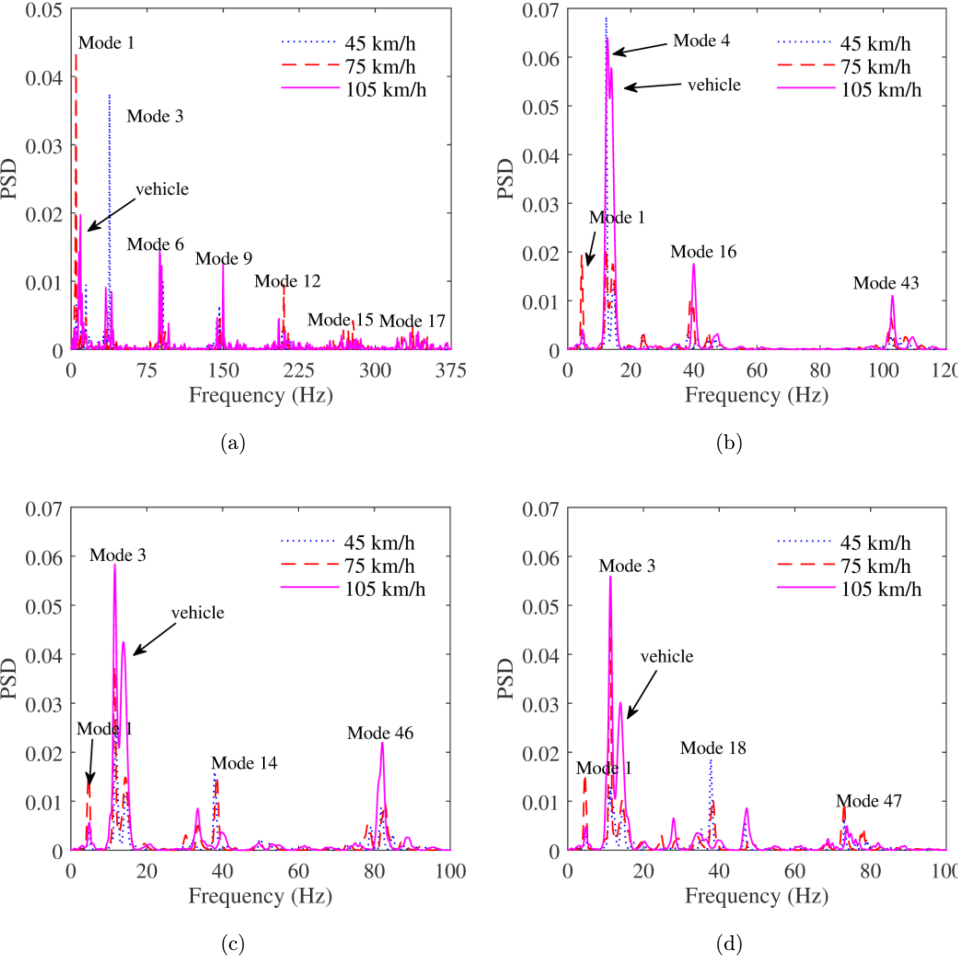
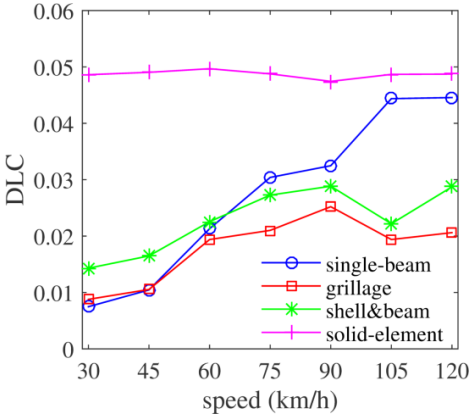


Fig. 10. (Color online) PSD spectra of the vertical accelerations at the mid-span of different bridge models under an average RSC: (a) Single-beam; (b) grillage; (c) shell-and-beam; and (d) solid-element.

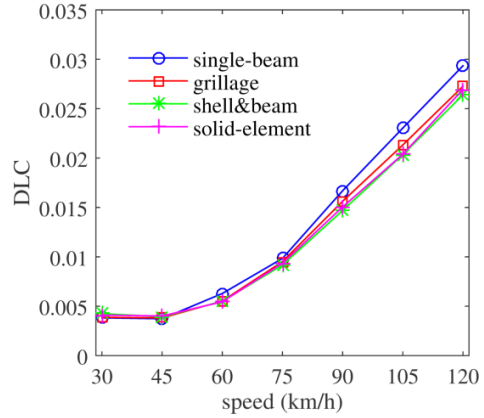
discrepancies of acceleration in the frequency domain between the single-beam and the other three bridge models are appreciable. For the single-beam model, periodic peaks can be observed in Fig. 10(a), which is quite different from the other three bridge models. Those peaks correspond to the symmetric vertical bending modes of the beam and their magnitudes diminish with the increase of the order of frequency.¹¹ A convergence test is conducted for the acceleration in which the number of modes used is gradually increased until the relative variation of the maximum acceleration is within 10%. The result shows that the modes with frequencies up to 340 Hz, which corresponds to the 17th mode, are needed. For the other three bridge models, on the other hand, several distinctive peaks can be identified. It is seen that the second peak, which is also the dominant peak, of the three models generally occurs around a frequency between 11 Hz and 12 Hz in Fig. 10(b)–10(d), which corresponds to the bidirectional flexural mode. This indicates the importance of the transverse modes in the symmetric loading cases once again. The third peak, which is close to the second peak, can be attributed to the second axle hopping mode (13.87 Hz) of the 3D SDM vehicle model. Meanwhile, as for the single-beam model, it can be seen that compared with the calculation of deflection and bending strain, more high-frequency modes are required to guarantee the accuracy of the calculated bridge acceleration. To be more specific, high peaks are still present at a high frequency around 103 Hz (43rd overall mode) for the grillage model, 83 Hz (46th overall mode) for the shell-and-beam model and 74 Hz (47th overall mode) for the solid-element model, as indicated in Fig. 10.

4.1.2. Contact forces

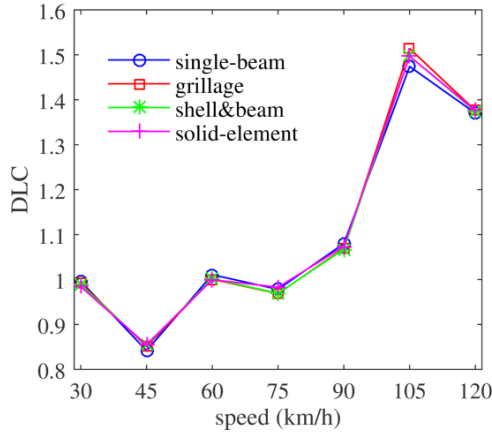
This sub-subsection only focuses on the effect of the bridge model on the contact forces while the difference in bridge responses due to different bridge models is discussed in other sections. Due to the fact that the forces are assumed to be constant in the moving-force model, which means that the DLC always equals to zero, only the other two vehicle models are discussed here. The rear axle, which is the heaviest axle of the vehicle, is used to calculate the DLC. Figure 11 shows the DLCs of two vehicle models with different bridge models under case 2. Different patterns of variation of DLC with the increase of vehicle speed are observed between the moving-mass model and the SDM vehicle model. The bridge models make a notable difference to the DLC when the moving-mass model is used. For the solid-element bridge model, the DLC almost remains a constant under the varying vehicle speed; while for the other three bridge models, the DLC varies significantly with the increase of the speed, generally following an ascending trend. This can be explained by examining the governing equation of motion for the moving-mass problem, where the coupling term in the stiffness matrix is presented as $v^2 \sum_{i=1}^k M_{vi} \{N_i\}^T \{N_{ixx}\}$ in Eq. (3.3).²⁴ This term is not only proportional to the square of vehicle speed, which indicates that the increase of vehicle speed distinctively enlarges the contact force, but also affected by $\{N_{ixx}\}$, the second-order derivative of the shape function, which



(a)



(b)



(c)

Fig. 11. (Color online) DLCs of two vehicle models with different bridge models under case 2: (a) Moving-mass vehicle model under perfectly smooth RSC; (b) SPC-SDM vehicle model under perfectly smooth RSC and FC condition; and (c) SPC-SDM vehicle model under poor RSC and FC condition.

depends on the type of element used in the bridge model. For the bridge with solid elements, the second-order derivative of the shape function, which has a tri-linear form, equals to zero. In contrast, the second-order derivative of the shape function for the other three bridge models, which has the form of cubic polynomial, is a linear function. Therefore, the DLC of the moving-mass model with the solid-element bridge model is less sensitive to the variation of the vehicle speed than those with the other bridge models. On the contrary, when the SDM vehicle model is used, the DLCs with different bridge models display a very similar pattern, as shown in Figs. 11(b) and 11(c).

4.2. Effect of the vehicle model

4.2.1. Moving-force, moving-mass and SPC-SDM vehicle models

In order to fairly compare the effects of different vehicle models on the dynamic responses of bridges, the RSC is initially assumed to be perfectly smooth. Furthermore, case 2 is chosen as the loading case in order to draw a fair comparison between the single-beam model and the other three bridge models. Figure 12 displays the IMs of the four bridge models under different vehicle models traveling at different speeds. The following can be observed from Fig. 12: (i) All IMs are relatively small due to the smooth RSC, although that the IMs of the single-beam model are slightly larger than those of the other models; and (ii) the IMs vary with vehicle speed and the difference of IMs between different vehicle models can be distinctive with the increase of the vehicle speed, which agrees with the previous findings.^{30,31}

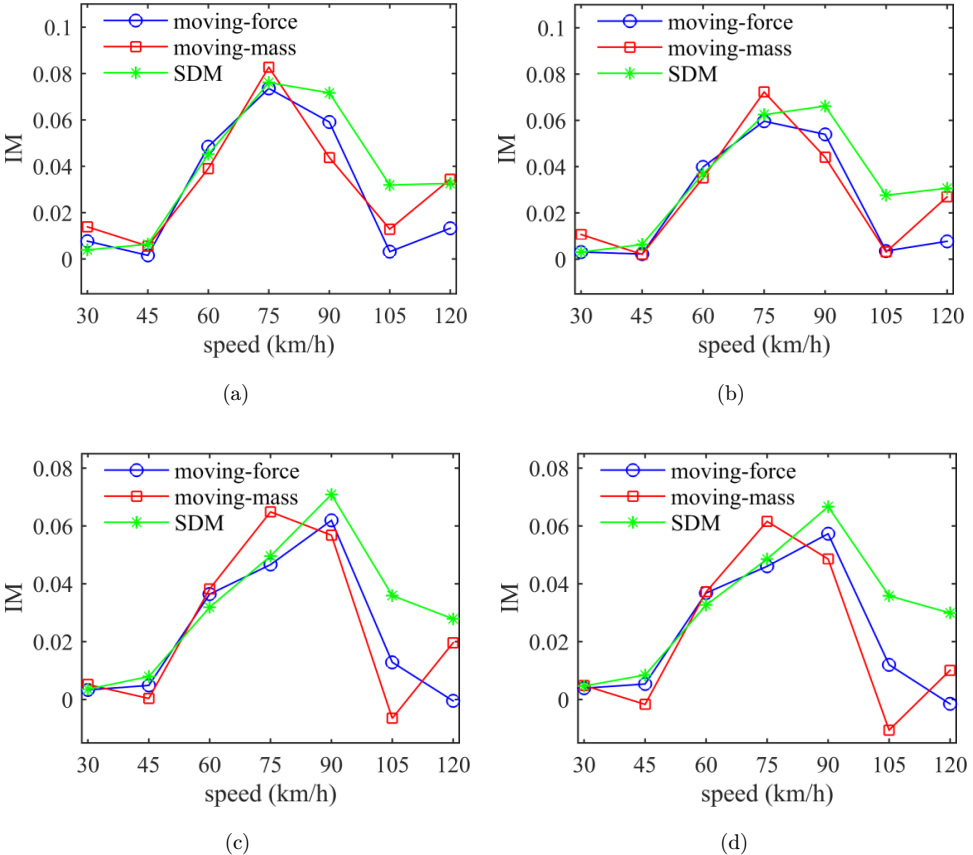


Fig. 12. (Color online) IMs of four bridge models under case 2 and perfectly smooth RSC: (a) Single-beam; (b) grillage; (c) shell-and-beam; and (d) solid-element.

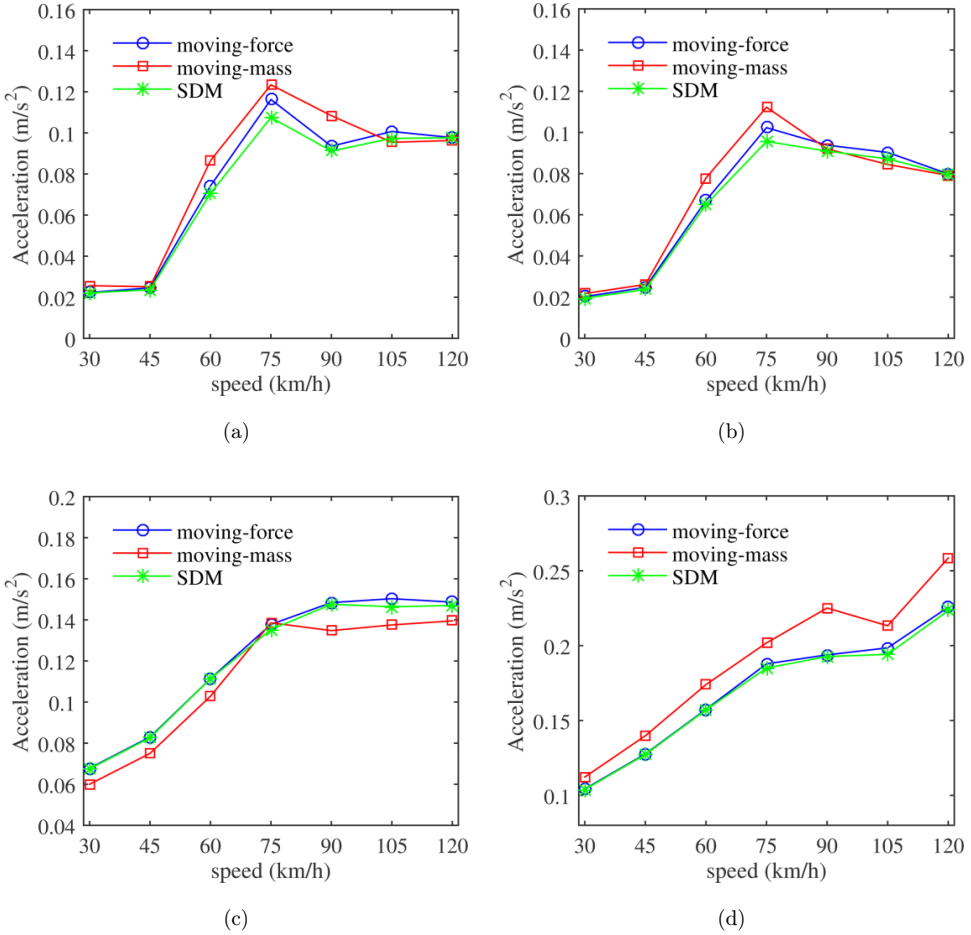
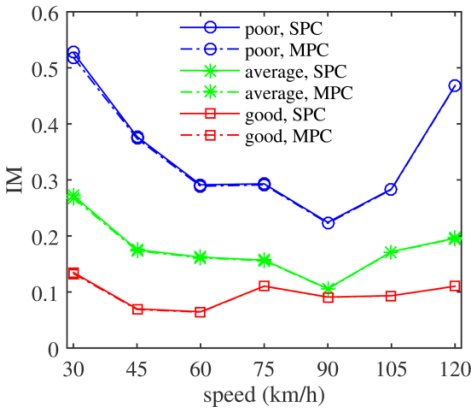


Fig. 13. (Color online) RMS values of vertical acceleration of the bridge models under case 2 and perfectly smooth RSC: (a) Single-beam; (b) grillage; (c) shell-and-beam; and (d) solid-element.

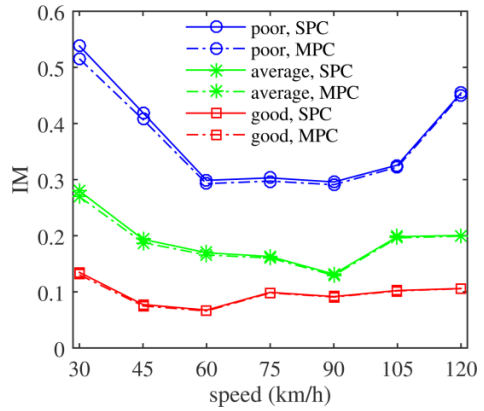
Depicted in Fig. 13 are the root-mean-square (RMS) values of vertical acceleration of different bridge models under case 2 with different vehicle models. It can be seen that the variation of bridge acceleration with vehicle speed for each particular bridge shows a similar trend among different vehicle models. However, different trends are observed between different bridge models and the RMS values of bridge acceleration also vary between different bridge models.

4.2.2. SPC-SDM and MPC-SDM vehicle models

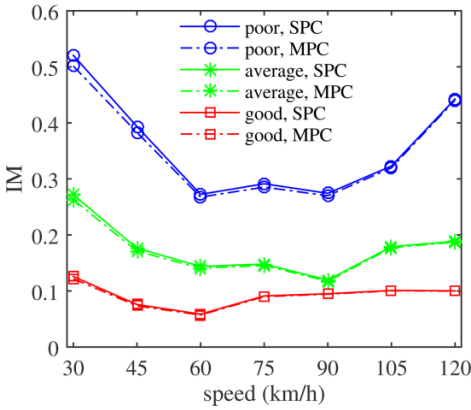
Figure 14 illustrates the IMs of the four bridge models under case 2 with SPC-SDM and MPC-SDM vehicle models. FC road roughness profiles are assumed. Similar variation trends of IM with vehicle speed can be observed among different bridge



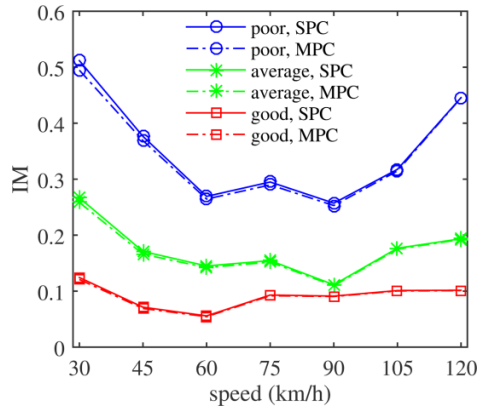
(a)



(b)



(c)



(d)

Fig. 14. (Color online) IMs of the four bridge models under case 2 with two SDM vehicle models: (a) Single-beam; (b) grillage; (c) shell-and-beam; and (d) solid-element.

models. In addition, it can be seen that the IMs induced by the SPC-SDM vehicle model are slightly larger than those induced by the MPC-SDM vehicle model.

Figure 15 shows the RMS values of the vertical acceleration of different bridge models under case 2 with SPC-SDM and MPC-SDM vehicle models. The acceleration of the single-beam model is smaller than the accelerations of the other models. By comparing Fig. 15 with Fig. 14, it can be observed that although the difference in the IMs induced by the SDM vehicle models with different tire models is negligible, the difference in the bridge accelerations can be considerable. The MPC tire model leads to smaller bridge acceleration compared with the SPC tire model, and the discrepancy increases when the RSC becomes worse, as illustrated by Fig. 15.

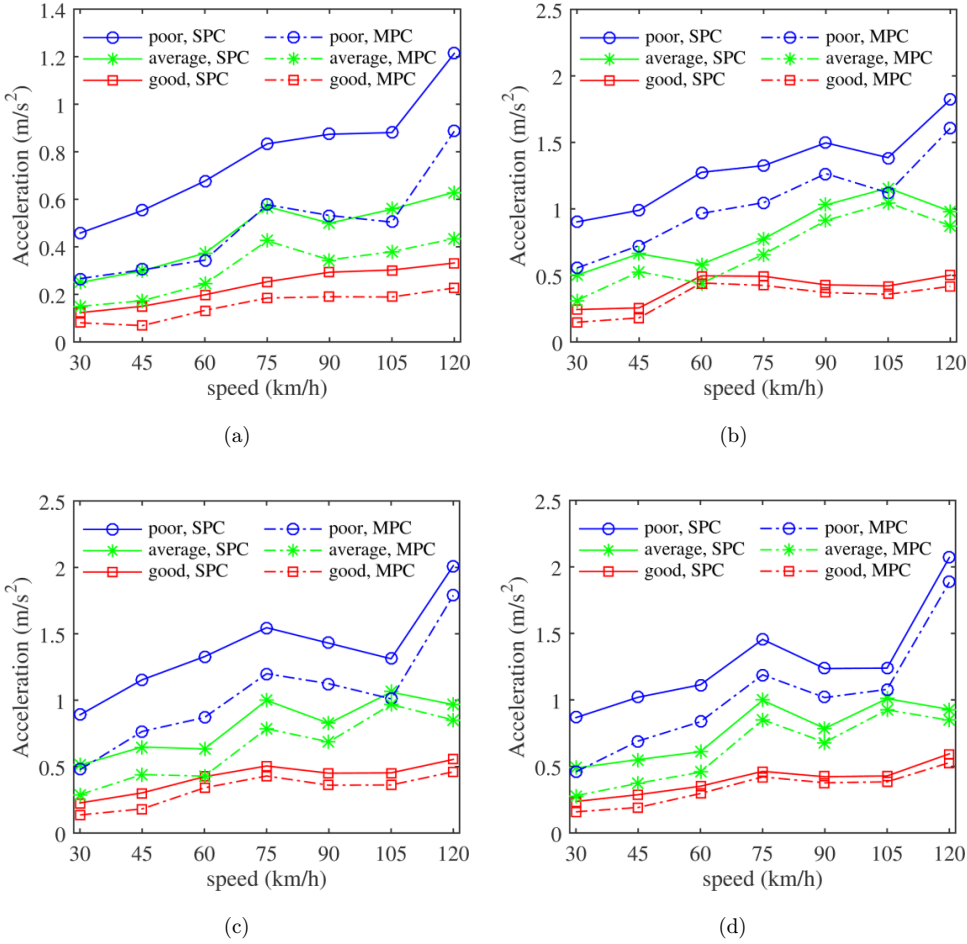


Fig. 15. (Color online) RMS values of vertical acceleration of different bridge models under case 2 with the SPC-SDM and MPC-SDM vehicle models: (a) Single-beam; (b) grillage; (c) shell-and-beam; and (d) solid-element.

4.3. Effect of the road roughness model

Figures 16 and 17 illustrate the IMs of deflection and the RMS values of the vertical acceleration of the three bridge models, respectively, under FC and PC roughness conditions. Significant difference can be easily observed between the results under the FC and PC conditions and this difference increases as the RSC becomes worse.

To further investigate the effects of correlation of the roughness profiles on bridge responses, the average IMs for different vehicle speeds are obtained and the IMs of different bridge models under different RSCs are summarized in Table 5. It can be seen that when the FC roughness condition is used, all IMs of the four bridge models under poor RSC exceed the value of 0.33, that is specified in the AASHTO LRFD

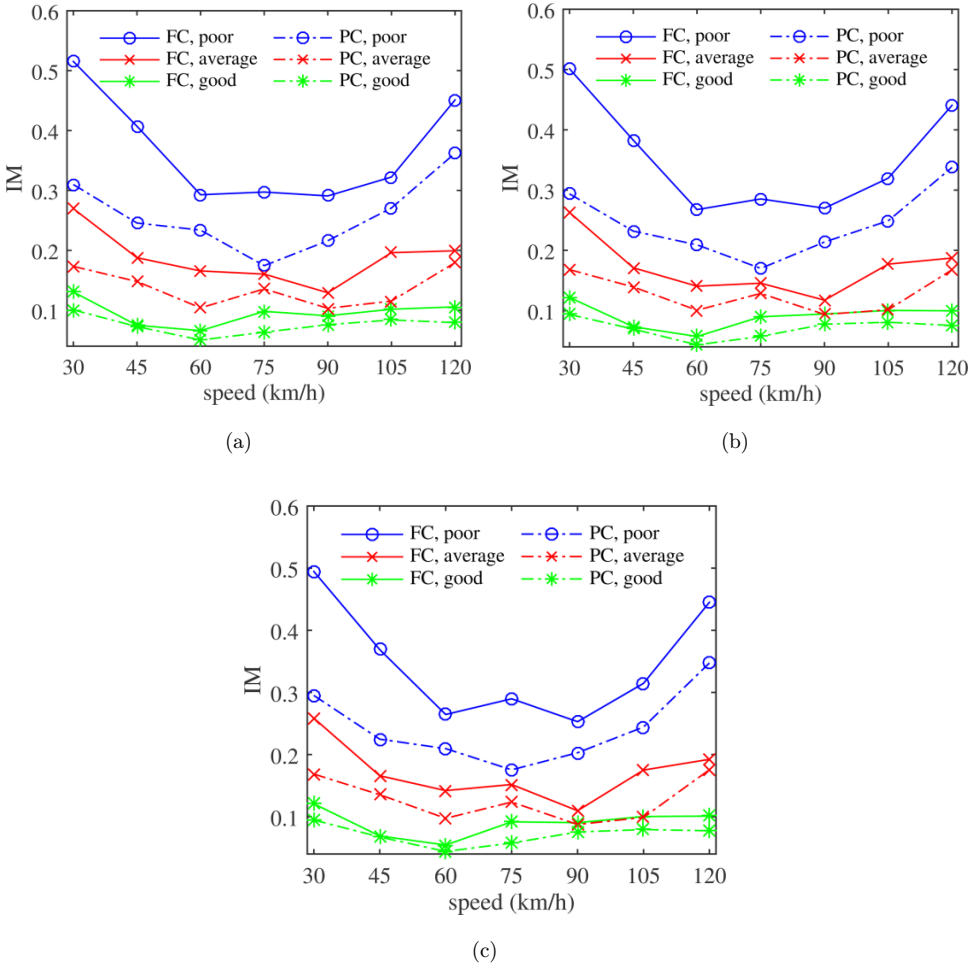


Fig. 16. (Color online) IMs of bridge deflection models under case 2 considering the correlation of road roughness profiles (MPC-SDM vehicle model): (a) Grillage; (b) shell-and-beam; and (c) solid-element.

code³²; while the results under the PC roughness condition are all below 0.33. Thus, using FC condition in the numerical simulation may overestimate the dynamic responses of the bridges. The IMs under the FC conditions can be greater than those under the PC conditions by more than 0.1 under poor RSC, as shown in Fig. 16 and Table 5.

5. Computational Efficiency

Table 6 lists the computation times of different VBI systems under case 2 and perfectly smooth RSC. It should be mentioned that based on the results and discussion in Sec. 4.1.1, the first 20 bridge vibration modes are used to calculate the responses of

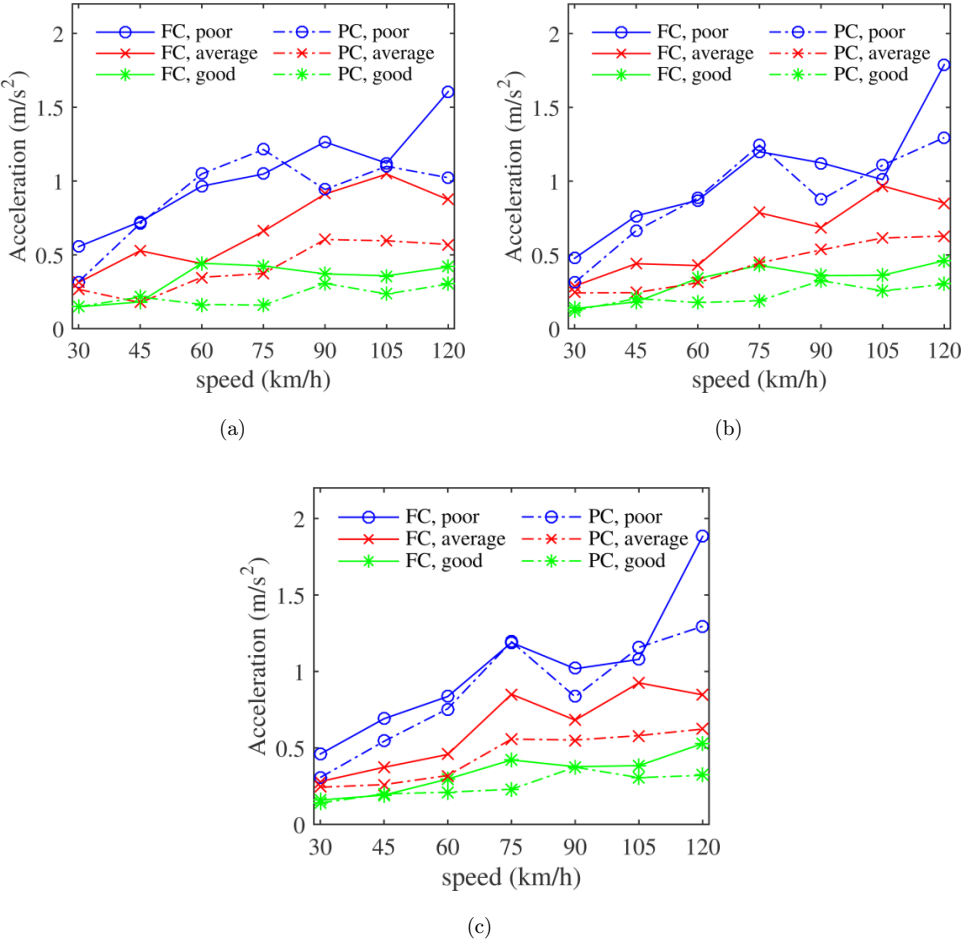


Fig. 17. (Color online) RMS values of bridge vertical acceleration under case 2 considering the correlation of road roughness profiles (MPC-SDM vehicle model): (a) Grillage; (b) shell-and-beam; and (c) solid-element.

Table 5. Average IMs of different bridge models under different RSCs (SPC-SDM vehicle model, case 2).

RSC	IM						
	Single-beam	Grillage		Shell-and-beam		Solid-element	
	Single track	FC	PC	FC	PC	FC	PC
Smooth	0.038	0.033	—	0.033	—	0.032	—
Very good	0.058	0.056	0.051	0.053	0.048	0.052	0.047
Good	0.096	0.097	0.076	0.093	0.072	0.091	0.072
Average	0.177	0.191	0.154	0.175	0.145	0.174	0.143
Poor	0.352	0.376	0.278	0.360	0.260	0.353	0.260

Table 6. Computation times of different VBI systems under case 2 and perfectly smooth RSC (60 km/h) (unit: s).

Bridge model	Vehicle model		
	Moving-force	Moving-mass	SDM
Single-beam	0.98	2.58	4.98
Grillage	2.02	5.98	21.35
Shell-and-beam	2.08	6.19	179.77
Solid-element	1.92	5.65	95.16

the single-beam bridge model while the first 60 modes are used for the other three bridge models. The time step adopted in the Newmark- β method is set to 0.001 s and the vehicle speed is set to 60 km/h. The MATLAB programs run on a PC with a 3.5-GHz 6-core CPU and 64-GB RAM. It can be seen that the single-beam bridge model requires the least computational effort under all circumstances due to its minimum number of DOFs, while the shell-and-beam bridge model is the least efficient due to the complex shape functions used in the calculation of the time-dependent terms when the moving mass and SDM vehicle models are used. Although the grillage model seems the most computationally-efficient model when used together with the SDM vehicle model, it needs more preprocessing work, i.e. calculating the moments of inertia and torsion constants of the equivalent longitudinal and transverse beams. The solid-element bridge model, on the other hand, can achieve a good balance between the accuracy and efficiency in this study. Meanwhile, as expected, the SDM vehicle model requires the most computational effort, followed by the moving-mass model, and then the moving-force model, due to the relative complexity of the coupled equations of motion for different vehicle models.

6. Concluding Remarks

A comprehensive comparative study on several existing VBI models is conducted. The theories of different VBI models are first presented. A simply-supported bridge is adopted and is modeled by a discretized Euler–Bernoulli beam, grillage, assemblage of shell and beam elements and solid elements, respectively. The vehicle is modeled as a moving-force, moving-mass and SDM model, respectively. Different tire models, namely the SPC and MPC tire models, and the correlation of the roughness profiles are also considered. The influence of different components of VBI models, including the bridge model, vehicle model and road roughness model, on the bridge responses is studied, and the results from different models are compared. The main conclusions are summarized as below:

- (i) Accurate prediction of different bridge responses requires a sufficient number of bridge vibration modes to be used in the numerical simulation. Low-order modes dominate the bridge deflection while bending strain and acceleration of the bridge are more sensitive to high-order modes than bridge deflection. It should

be noted that even under symmetric loading conditions, the contribution of the transverse modes to the bridge displacement and acceleration can be significant.

- (ii) The grillage, shell-and-beam and solid-element bridge models yield similar deflections with small difference under the vehicle loading considered in this study. It is found that despite the neglect of the lateral distribution of the vehicle load, the single-beam model can still be used to predict the IMs of the bridge under the symmetric loading without introducing excessive deviations. Meanwhile, the predicted bridge acceleration varies among different bridge models. It is noteworthy that the shape function of the bridge deck elements plays a critical role in calculating the contact force when using the moving-mass vehicle model.
- (iii) When RSC is smooth or very good, different vehicle models (moving-force, moving-mass and SDM models) yield slight discrepancy in the predicted bridge deflection at low vehicle speeds. Nonetheless, this difference can become appreciable at high vehicle speeds.
- (iv) The correlation of the roughness profiles can have a significant influence on the VBI. Assuming full correlation of the road roughness profiles will yield larger bridge dynamic responses.
- (v) The single-beam bridge model requires the minimum computational effort, while the shell-and-beam model is the least efficient due to the complex shape functions used in the calculation. The grillage bridge model is computationally-efficient but needs more preprocessing work for determining the parameters of the model. The solid-element bridge model can achieve a good balance between the accuracy and efficiency.

Acknowledgments

The authors gratefully acknowledge the financial support provided by the National Natural Science Foundation of China (Grant Nos. 51208189 and 51478176); and Excellent Youth Foundation of Hunan Scientific Committee (Grant No. 14JJ1014).

References

1. Y. B. Yang and B. H. Lin, Vehicle–bridge interaction analysis by dynamic condensation method, *J. Struct. Eng., ASCE* **121**(11) (1995) 1636–1643.
2. Y. B. Yang and Y. S. Wu, A versatile element for analyzing vehicle–bridge interaction response, *Eng. Struct.* **23**(5) (2001) 452–469.
3. S.-H. Yin, Vibration of a simple beam subjected to a moving sprung mass with initial velocity and constant acceleration, *Int. J. Struct. Stab. Dyn.* (2015), doi: 10.1142/S0219455414501090.
4. D. Z. Huang, T. L. Wang and M. Shahawy, Impact studies of multigirder concrete bridges, *J. Struct. Eng., ASCE* **119**(8) (1993) 2387–2402.
5. E. J. O’Brien, D. Cantero, B. Enright and A. González, Characteristic dynamic increment for extreme traffic loading events on short and medium span highway bridges, *Eng. Struct.* **32**(12) (2010) 3827–3835.

6. J. Oliva, J. M. Goicolea, P. Antolín and M. Á. Astiz, Relevance of a complete road surface description in vehicle–bridge interaction dynamics, *Eng. Struct.* **56** (2013) 466–476.
7. L. Deng and C. S. Cai, Development of dynamic impact factor for performance evaluation of existing multi-girder concrete bridges, *Eng. Struct.* **32**(1) (2010) 21–31.
8. X. M. Shi, C. S. Cai and S. R. Chen, Vehicle induced dynamic behavior of short-span slab bridges considering effect of approach slab condition, *J. Bridge Eng., ASCE* **13**(1) (2008) 83–92.
9. A. González, P. Rattigan, E. J. O'Brien and C. Caprani, Determination of bridge lifetime dynamic amplification factor using finite element analysis of critical loading scenarios, *Eng. Struct.* **30**(9) (2008) 2330–2337.
10. H. Y. Li, J. Wekezer and L. Kwasniewski, Dynamic response of a highway bridge subjected to moving vehicles, *J. Bridge Eng., ASCE* **13**(5) (2008) 439–448.
11. Y. B. Yang and C. W. Lin, Vehicle–bridge interaction dynamics and potential applications, *J. Sound Vib.* **284**(1–2) (2005) 205–226.
12. Y. B. Yang and J. D. Yau, Vehicle–bridge interaction element for dynamic analysis, *J. Struct. Eng., ASCE* **123**(11) (1997) 1512–1518.
13. L. Ding, H. Hao and X. Q. Zhu, Evaluation of dynamic vehicle axle loads on bridges with different surface conditions, *J. Sound Vib.* **323**(3–5) (2009) 826–848.
14. Y. B. Yang, C. H. Chang and J. D. Yau, An element for analysing vehicle–bridge systems considering vehicle's pitching effect, *Int. J. Numer. Methods Eng.* **46**(7) (1999) 1031–1047.
15. H. Zeng and C. W. Bert, Dynamic amplification of bridge/vehicle interaction: A parametric study for a skewed bridge, *Int. J. Struct. Stab. Dyn.* **03**(01) (2003) 71–90.
16. X. F. Yin, C. S. Cai, Z. Fang and L. Deng, Bridge vibration under vehicular loads: Tire patch contact versus point contact, *Int. J. Struct. Stab. Dyn.* **10**(3) (2010) 529–554.
17. K. C. Chang, F. B. Wu and Y. B. Yang, Disk model for wheels moving over highway bridges with rough surfaces, *J. Sound Vib.* **330**(20) (2011) 4930–4944.
18. L. Kwasniewski, H. Y. Li, J. Wekezer and J. Malachowski, Finite element analysis of vehicle–bridge interaction, *Finite. Elem. Anal. Des.* **42**(11) (2006) 950–959.
19. C. H. Liu, D. Z. Huang and T. L. Wang, Analytical dynamic impact study based on correlated road roughness, *Comput. Struct.* **80**(20–21) (2002) 1639–1650.
20. International Organization for Standardization (ISO), ISO 8608: Mechanical vibration — Road surface profile — Report of measured data, Geneva (1995).
21. American Association of State Highway and Transportation Officials (AASHTO), Standard Specifications for Highway Bridges, Washington, DC (2002).
22. G. H. Tan, G. H. Brameld and D. P. Thambiratnam, Development of an analytical model for treating bridge–vehicle interaction, *Eng. Struct.* **20**(1–2) (1998) 54–61.
23. T. H. T. Chan and C. O'Connor, Vehicle model for highway bridge impact, *J. Struct. Eng., ASCE* **116**(7) (1990) 1772–1793.
24. J. R. Rieker and M. W. Trethewey, Finite element analysis of an elastic beam structure subjected to a moving distributed mass train, *Mech. Syst. Signal Process.* **13**(1) (1999) 31–51.
25. K. Liu, N. Zhang, H. Xia and G. De Roeck, A comparison of different solution algorithms for the numerical analysis of vehicle–bridge interaction, *Int. J. Struct. Stab. Dyn.* **14** (02) (2014) 1350065.
26. Y. Pala and M. Reis, Dynamic response of a cracked beam under a moving mass load, *J. Eng. Mech., ASCE* **139**(9) (2013) 1229–1238.
27. L. Deng and C. S. Cai, Identification of dynamic vehicular axle loads: Demonstration by a field study, *J. Vib. Control* **17**(2) (2010) 183–195.

28. M. Majka and M. Hartnett, Effects of speed, load and damping on the dynamic response of railway bridges and vehicles, *Comput. Struct.* **86**(6) (2008) 556–572.
29. L. Deng, Y. Yu, Q. L. Zou and C. S. Cai, State-of-the-art review of dynamic impact factors of highway bridges, *J. Bridge Eng., ASCE* **20**(5) (2015) 04014080.
30. H. P. Lee, Dynamic response of a beam with a moving mass, *J. Sound Vib.* **191**(2) (1996) 289–294.
31. F. T. K. Au, J. J. Wang and Y. K. Cheung, Impact study of cable-stayed bridge under railway traffic using various models, *J. Sound Vib.* **240**(3) (2001) 447–465.
32. American Association of State Highway and Transportation Officials (AASHTO), LRFD Bridge Design Specifications, Washington, DC (2012).